



Application of nickel-doped graphene nanotubes to modified GCE as a sensitive electrochemical sensor for the antipsychotic drug clozapine in spiked human blood serum samples

Mohammad Hossein Ghanbari^{1,2} · Zahra Norouzi³ · Anahid Amiri⁴

Received: 5 August 2022 / Accepted: 2 January 2023 / Published online: 14 January 2023
© The Author(s) 2023

Abstract

Clozapine (CLZ) is one of the most vital medications for managing schizophrenia, and the timely measurement of CLZ levels has been recognized as an obstacle to the wider use of CLZ. Herein, for the first time, nickel-doped graphene nanotubes (Ni@GRNT) were used to construct an electrochemical CLZ sensor by drop coating Ni@GRNT suspension on a glassy carbon electrode. The Ni@GRNT was synthesized and characterized using X-ray diffraction, scanning electron microscopy, and energy-dispersive X-ray spectroscopy. The electrochemical behavior and influence of different physicochemical factors of sensing electrodes were investigated by using cyclic voltammetry, EIS technique, and differential pulse voltammetry techniques. Also, the catalytic rate constant (k_{cat}) and the transfer coefficient (α) were calculated. The modified electrode illustrated satisfactory linear range, detection limit (LOD), reusability, and reproducibility results. At optimal experimental conditions, measurements can be performed at a broad linear dynamic range of 0.3 nmol L^{-1} – $60.0 \text{ } \mu\text{mol L}^{-1}$ CLZ and with a LOD of 0.1 nmol L^{-1} . The sensitivity value was estimated to be $3.06 \text{ } \mu\text{A } \mu\text{mol L}^{-1} \text{ cm}^{-2}$. Ultimately, this platform was successfully used for CLZ sensing in spiked human blood serum and tablet samples with an accuracy of $> 93\%$.

✉ Mohammad Hossein Ghanbari
ghanbari_khat@yahoo.com

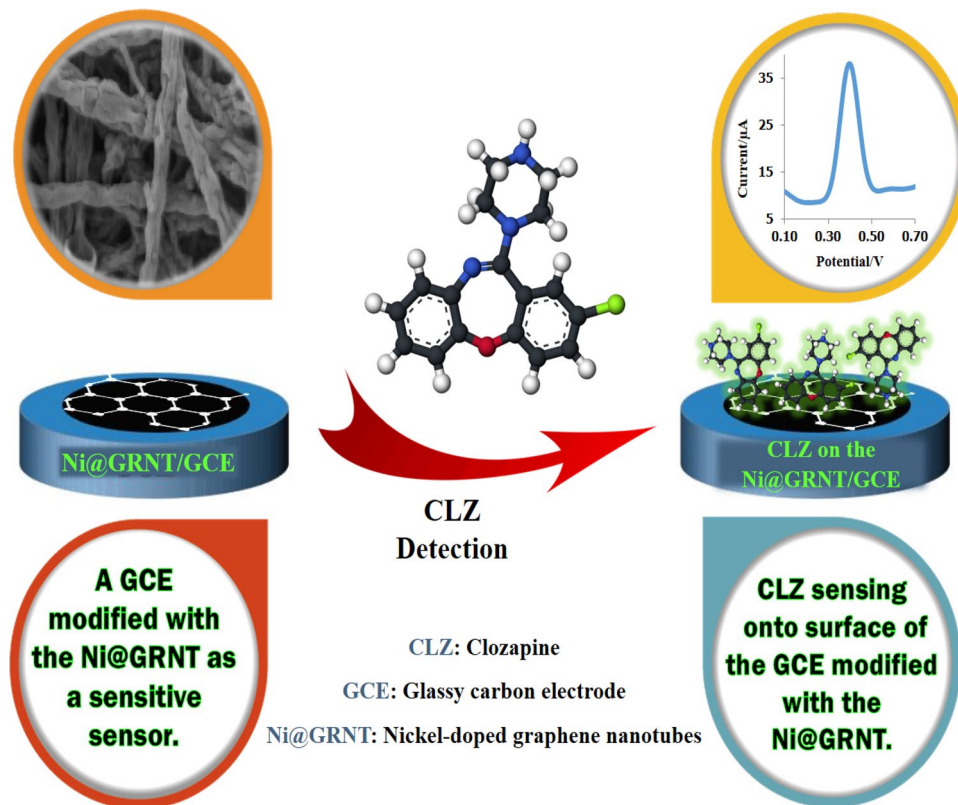
¹ Faculty of Chemistry, Kharazmi University, 15719-14911, Tehran, Iran

² Ernst-Berl-Institute for Technical Chemistry and Macromolecular Science, Technische Universität Darmstadt, Alarich-Weiss-Straße 8, 64287 Darmstadt, Germany

³ Faculty of Chemistry, University of Kashan, 87317-51167, Kashan, Iran

⁴ Physics of Surfaces, Institute of Materials Science, Technische Universität Darmstadt, Alarich-Weiss-Str. 2, 64287 Darmstadt, Germany

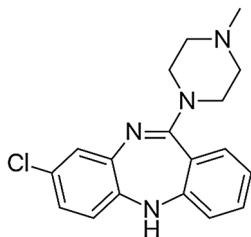
Graphical abstract



Keywords Clozapine · Antipsychotic drug · Electrochemical sensor · Nickel-doped graphene nanotubes · Nanotubes · Electrode modification

Introduction

Clozapine (CLZ), $C_{18}H_{19}ClN_4$, is a standard antipsychotic drug and one of the most effective treatments for tenacious schizophrenia, controlling violent behaviors and suicidal or similar perturbations. The chemical structure of CLZ is shown below:



Studies demonstrate that 30–60% of patients with treatment-resistant schizophrenia may respond to this valuable drug. However, despite its widespread use, CLZ also poses adverse side effects and controlling its dosage value is therefore crucial [1]. Reliable and accurate techniques such as chromatography and spectrophotometry have been universally used for the quantitative analysis of CLZ in

variant formulations as well as in biological samples [2–4]. However, these methods also have disadvantages, e.g., the low sensitivity in spectroscopy and the high-cost, tedious process and often complex sample preparation in high-performance liquid chromatography (HPLC). The use of electrochemical sensors therefore presents an attractive alternative for the detection and quantification of CLZ. Moreover, using relatively non-toxic and safe substances, the possibility of miniaturized in vivo electroanalytical sensors can be realized to provide rapid, simple, highly sensitive and cost-effective means for monitoring CLZ levels [5–8]. A number of electrochemical techniques, such as amperometry and voltammetry, have already been employed for the determination of the CLZ level [9, 10]. Nonetheless, some of them suffer from high detection limits, low sensitivity and selectivity or low linear concentration range. As regards the challenge of sustaining serum levels of the CLZ in a secure therapeutic range (1–3 μM) [11], a reliable and responsive method for the measurement of this drug is important.

Providing an efficient platform to realize a stable electrochemical response may be a significant element for the fabrication of an excellent sensitive electrochemical sensor.

The glassy carbon electrode (GCE) remains to be an appealing choice due to its simple fabrication, wide potential range, low residual current and simple surface regeneration. Introducing nanostructures or nanomaterials on the other hand can modify and improve the activity of electrochemical sensors. Graphene, for instance, due to its excellent conductivity and interesting catalytic activity, has been incorporated into various sensing platforms [12, 13]. However, the slow direct electron transfer from graphene layers to the unmodified electrode surface results in a high limit of detection (LOD) and low sensitivity. Thus, electrode surface modification becomes imperative for the production of high-quality graphene-based electrochemical sensors. Further, extensive research is being done to look at the application of different nanomaterials like metallic nanoparticles, quantum dots and a few nanocomposites containing carbon nanostructures in order to enhance the electrochemical sensing properties [14–16].

Due to their excellent electrical conductivity, mechanical strength, and the enormous specific area, carbon nanotubes (CNTs) and graphene have been employed as active electrodes for supercapacitors. On the other hand, aggregate formation in CNTs and/or graphene plates mostly resulted in flexible supercapacitors with a comparatively indistinct performance [17, 18]. Further progress in carbon nanotube-on-graphene (nanotube@graphene) hybrids has been achieved by growing CNTs vertically on graphene sheets [19–23]. The formed nanotube@graphene hybrids possessed a typical 3D structure, which may efficiently prevent aggregation between them, resulting in an increased total surface area [24, 25]. In addition, the seamlessly connected nanotube@graphene hybrids exhibited an Ohmic contact at the junction between the graphene and the nanotubes, resulting in a fast charge transfer from the graphene to the nanotubes [24, 25]. Thus, owing to their resulting excellent electrical property and enormous surface area, the seamlessly connected nanotube@graphene hybrids can be used as effective electrodes for electronic devices, such as high-performance supercapacitors [24, 25] and electrochemical sensors [26–29]. Metal–nanoparticle composites containing graphene and carbon nanotubes with high stability and catalytic power are explored to improve electrocatalytic activity and have a high active surface area [30–33].

In the present study, we synthesized nickel-doped graphene nanotubes (Ni@GRNT) to scale back the clustering effect of nanoparticles and maintain the catalytic activity of such hybrid materials. Ni@GRNT were then deposited onto GCE (Ni@GRNT/GCE) and were evaluated for its performance for the first time as a CLZ sensor in spiked human blood serum samples, via the electrocatalytic oxidation of CLZ.

The properties and characterization of the modified electrode as a CLZ sensor were studied using electrochemical and materials characterization techniques. Further,

we demonstrate here that the fabricated Ni@GRNT/GCE provides a low-cost, portable, rapid and sensing platform option.

Experimental section

Materials, reagents, samples, and apparatus

CLZ, 3,3,5,5'-tetramethylbenzidine (TMB), oxalic acid, nickel chloride, melamine, sulfuric acid (H_2SO_4), chloroplatinic acid, sodium borohydride, sodium hydroxide (NaOH), hydrochloric acid (HCl), and all other materials were purchased from Merck (<http://www.merck.com>), Sinopharm Chemical Reagent (<http://en.reagent.com.cn/>) or Sigma-Aldrich (<http://www.sigmaaldrich.com>) companies. Materials and reagents were of analytical grade and used without further purification. High-purity water (using Ultrapure Water System (Smart-2-Pure, TKACo, Germany)) was used for all experiments in this study. Phosphate buffer solutions (PBS) and acetate buffer solutions (ABS) were used to adjust the pH as supporting electrolytes. The cold field emission scanning electron microscope (FESEM) used was a JSM-6700F (Japan). The X-ray diffraction (XRD) patterns of the synthesized nanostructure were obtained using a Philips, X'Pert Pro (Netherlands). Electrochemical measurements were taken using a Palm Sens Em state 3 + Potentiostat (Netherlands). The differential pulse voltammetry (DPV) experiments were performed at $E_{\text{step}} = 5 \text{ mV}$, $E_{\text{pulse}} = 60 \text{ mV}$, $t_{\text{pulse}} = 0.02 \text{ s}$ and with a scan rate of 0.1 V s^{-1} . A redox probe was prepared using a solution containing $5.0 \text{ mM K}_3\text{Fe}(\text{CN})_6/\text{K}_4\text{Fe}(\text{CN})_6$ and 0.1 M KCl (1:1). An Ag/AgCl/KCl (3.0 M) reference electrode, a Pt wire counter electrode (Azar Electrode, Iran), and a glassy carbon working electrode (unmodified or modified) (geometric surface area = 0.03 cm^2) were used to build a three-electrode system for the electrochemical experiments. A pH/mV meter (Bel PHS3-BW (Italy)) was used for pH studies. All experiments were carried out at ambient temperature.

The CLZ tablets were obtained from the pharmaceutical company of Tehran Chemistry (<http://www.tehrandarou.com>), whereas the human blood serum samples were from the Blood Transfusion Organization (<http://www.tbtc.ir>) in Tehran, Iran.

Preparation of spiked human blood serum samples and (solution from) CLZ tablet

Spiked human blood serum samples were prepared from CLZ tablets and human blood serum samples. First, the serum samples were diluted with 0.1 mol L^{-1} PBS to a ratio of 1:20 and then set aside. Then, a stock solution of CLZ was prepared by dissolving powdered 25.0 mg CLZ (~ 10

tablets) in $0.1 \text{ mol L}^{-1} \text{ HNO}_3$ to a final concentration of $0.01 \text{ mmol L}^{-1} \text{ CLZ}$. To remove undissolved impurities, the solution was also filtered. The stock solution was then used to prepare solutions of different CLZ concentrations by further dilution with $0.1 \text{ mol L}^{-1} \text{ PBS}$. These solutions were then used to spike the diluted human blood serum samples resulting in serum samples with different concentrations of CLZ. These CLZ-spiked serum samples were then used for DPV measurements with the Ni@GRNT.

Preparation of nickel-doped graphene nanotubes (Ni@GRNT)

The Ni@GRNT was synthesized based on the Bao method [34]. Briefly, 1.57 g oxalic acid was added into 40.0 mL of high-purity water. Then, 1.26 g melamine and 10.0 mL 0.25 mol L^{-1} nickel (II) chloride were added to this solution. To form a homogeneous emulsion, the mixture was then stirred for 45 min at room temperature and then subsequently refluxed at $80 \text{ }^\circ\text{C}$ for 12 h. During the synthesis, Ni^{2+}

Scheme 1 Fabrication of nickel-doped graphene nanotubes grafted onto glassy carbon electrode (Ni@GRNT/GCE) as an electrochemical sensor for clozapine (CLZ)

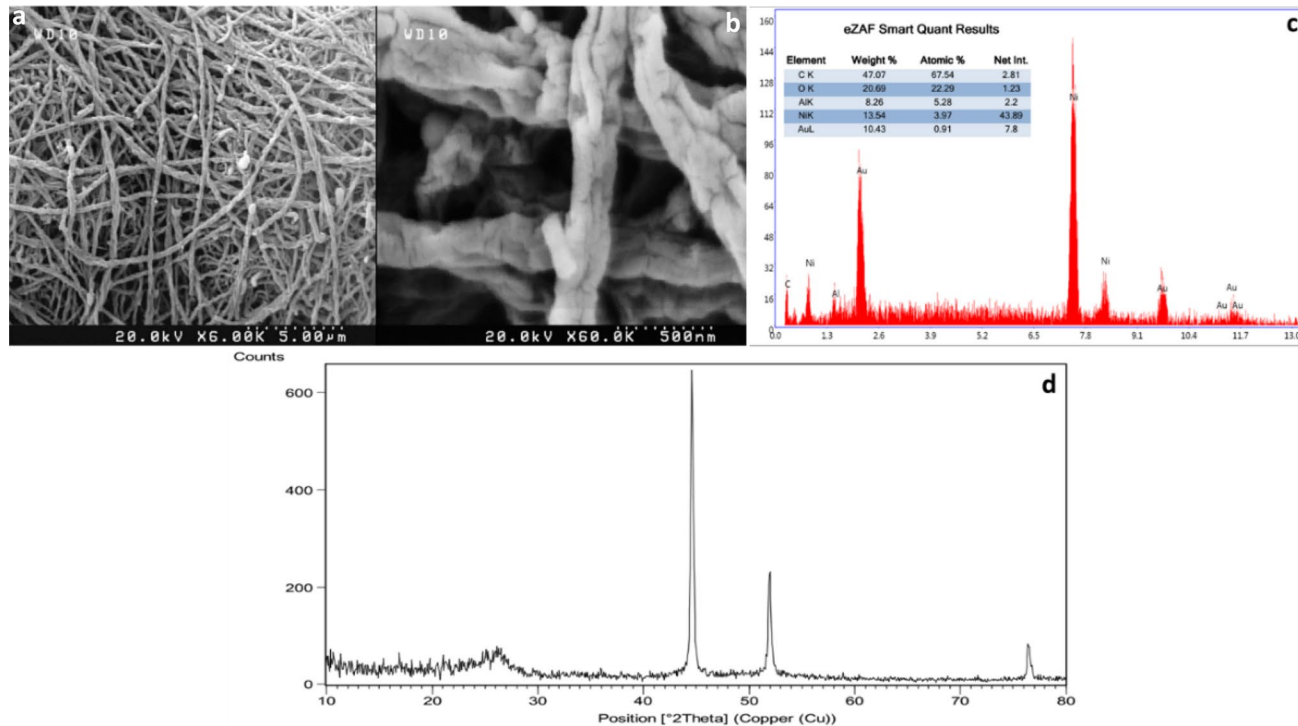
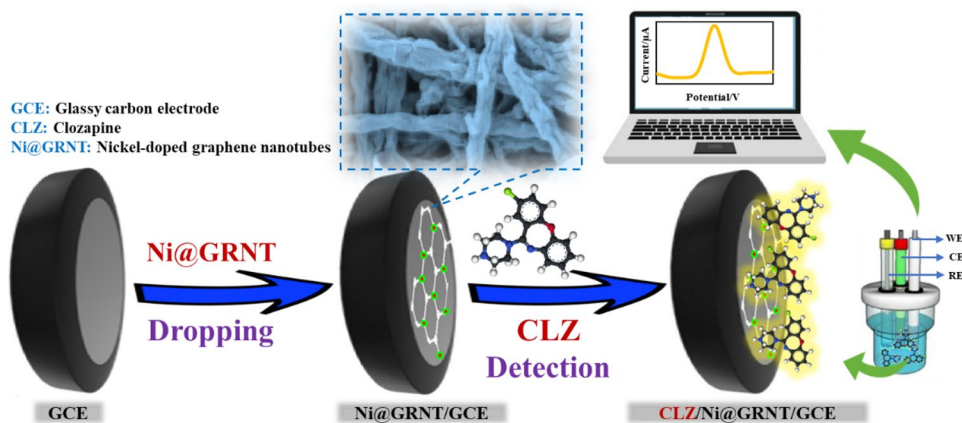


Fig. 1 SEM images of Ni@GRNT (a, b), the recorded EDX spectrum Ni@GRNT (c), and the XRD diffractogram of the prepared Ni@GRNT (d)

is homogeneously dispersed via chelation with the oxalic-acid-treated melamine composites. The emulsion was then filtered to obtain the filter cake, which was then dried and powdered. The resulting powder was then heated up at a rate of $5\text{ }^{\circ}\text{C min}^{-1}$ until it reached $900\text{ }^{\circ}\text{C}$, at which it was then held constant for 120 min in N_2 . The resulting black fluffy particles were then dispersed in $0.5\text{ mol L}^{-1}\text{ H}_2\text{SO}_4$ at $80\text{ }^{\circ}\text{C}$ for 8 h to produce the Ni@GRNT.

Fabrication of the Ni@GRNT/GCE

The GCE was polished using $0.05\text{-}\mu\text{m}$ alumina powder slurry and then sonicated in deionized (DI) water for 3 min to remove surface contamination. The GCE was then dried at $25\text{ }^{\circ}\text{C}$ in the air prior to use. Afterward, 1.0 mg of the Ni@GRN was added to 10.0 mL ethanol and the mixture was sonicated for 45 min. Ni@GRNT/GCE is produced by dropping $4.0\text{ }\mu\text{L}$ of the mixture onto the polished GCE and allowing the electrodes to dry in the air. These electrodes were stored at room temperature prior to use. The fabrication process of the sensor is also shown in Scheme 1. These sensor electrodes were then subjected to various electrochemical measurements to investigate their electrochemical behavior.

Results and discussion section

Characterization of the Ni@GRNT

The morphology and structure of the synthesized Ni@GRNT were investigated using a field-emission scanning electron microscope (FE-SEM). Figure 1a shows the entwined Ni@GRNT nanostructures, which form a connected conductive network. At higher magnification (Fig. 1b), the smooth

surface of the Ni@GRNT can be seen. This morphology composed of irregular lumps from seemingly interwoven strands of Ni@GRNT, and without forming any agglomerates, provides a high-surface area electrode for effective electrochemical measurements. Furthermore, in Fig. 1c, the energy-dispersive X-ray (EDX) spectrum confirms the presence of the elements Ni, O and C in the Ni@GRNT. Additionally, the crystal structure and phase purity of the Ni@GRNT are examined by XRD analysis, and the diffraction peaks are shown at 26° , 44° , 53° and 77° (Fig. 1d).

Electrochemical behavior of the Ni@GRNT as a CLZ sensor

To investigate the electrochemical behavior of the Ni@GRNT/GCE, cyclic voltammograms (CVs) of the modified and bare GCE were recorded in a redox probe containing 0.1 M PBS , $5.0\text{ mmol L}^{-1}\text{ K}_3\text{Fe}(\text{CN})_6/\text{K}_4\text{Fe}(\text{CN})_6$ and $0.1\text{ mol L}^{-1}\text{ KCl}$ (1:1) at a scan rate of 100 mV s^{-1} (Fig. 2a). The higher current of the Ni@GRNT/GCE compared to that of the unmodified GCE shows that the addition of Ni@GRNT increases the current signal needed in producing an effective sensor. This increase in current is likely due to the Ni@GRNT serving as a bridge to accelerate the electron transfer between the redox probe and the GCE surface. As such, we also performed EIS to further characterize the electron transfer properties of the Ni@GRNT/GCE. The charge transfer resistance, R_{ct} , can be used to estimate the kinetics of the redox probe at the (modified) GCE interface and investigate the probe attachment on the Ni@GRNT/GCE [16, 17]. Indeed, the Nyquist plots (Fig. 2b) show the smaller R_{ct} of Ni@GRNT/GCE ($280\text{ }\Omega$), compared to that of the unmodified GCE ($750\text{ }\Omega$). This reduction of the R_{ct} value can be attributed to the increased surface area and better conductivity with the addition of the Ni@GRNT nanostructures.

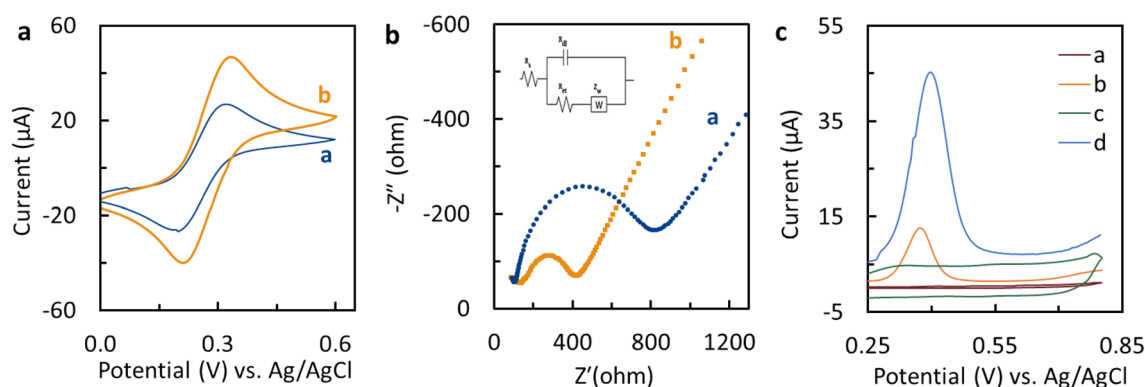


Fig. 2 The recorded **a** CV curves and **b** Nyquist plots for the **a** bare GCE and **b** Ni@GRNT/GCE in $5.0\text{ mmol L}^{-1}\text{ [Fe}(\text{CN})_6]^{3-/4-}$ and $0.1\text{ mol L}^{-1}\text{ KCl}$ (1:1) as a redox probe at a scan rate of 100 mV s^{-1} . Inset: An equivalent circuit for the fitted Nyquist plots. **c** The

recorded CVs in the absent of the CLZ in 0.1 M PBS ($\text{pH}=7.0$) for **a** bare GCE and **c** Ni@GRNT/GCE, and DPVs of 0.2 mmol L^{-1} CLZ for the **b** bare GCE and **d** Ni@GRNT/GCE in $0.1\text{ mol L}^{-1}\text{ PBS}$ ($\text{pH}=7.0$)

The noticeable increase of the current with the Ni@GRNT/GCE shows that the Ni@GRNT effectively modified the GCE. Consequently, both the CV and EIS confirm the successful fabrication of the Ni@GRNT as an electrochemical sensor.

The electrochemically active surface area (A) of the Ni@GRNT/GCE and unmodified GCE can also be determined by performing CV at various scan rates according to the Randles–Sevcik equation [35]. From the redox peaks in the CV plots of the bare and modified GCE in the redox probe, the value of A for Ni@GRNT/GCE and the unmodified GCE were determined to be 0.54 cm^2 and 0.06 cm^2 , respectively. These findings show the apparent increase in the surface area of the GCE upon modification with Ni@GRNT.

Improving the modified Ni@GRNT/GCE

To evaluate the performance of the Ni@GRNT/GCE in the detection and determination of CLZ, its electrocatalytic behavior against the unmodified GCE, in the presence of 0.2 mmol L^{-1} CLZ in 0.1 mol L^{-1} PBS ($\text{pH}=7.0$), was studied by DPV (Fig. 2c). Overall, the Ni@GRNT/GCE produces a larger peak current and a more positive E_p value in comparison with the unmodified GCE. This behavior can be attributed to the interconnected conductive structure and larger surface area of the Ni@GRNT/GCE. In the absence

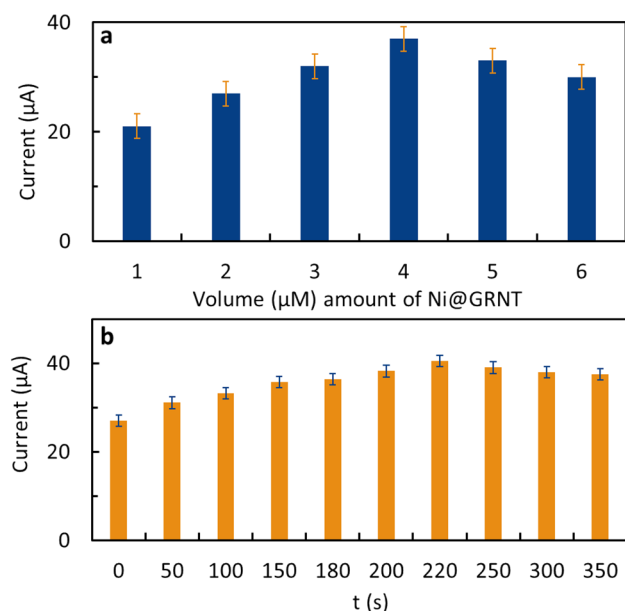


Fig. 3 **a** The effect of the amount of Ni@GRNT on the electrode modification process based on the measured current response. Here, we used different volumes of 1 mg/mL Ni@GRNT solutions (1, 2, 3, 4, 5 and $6 \text{ }\mu\text{L}$) containing 0.1 mmol L^{-1} CLZ. **b** The effect of the adsorption time on current response of the modified electrode from 0 to 350 s. Here, we measured in a solution containing 0.1 mmol L^{-1} CLZ in 0.1 mol L^{-1} PBS at $\text{pH}=7.0$ (Number of replicates = 4)

of the CLZ, the Ni@GRNT/GCE shows an increased capacitive current compared to the bare GCE. To maximize the signal for the determination of CLZ on the Ni@GRNT/GCE surface, several vital analytical parameters were optimized which are described in the following sections.

Optimization of the Ni@GRNT amount and accumulation time

The initial amount of the Ni@GRNT deposited onto the GCE surface can also influence the signals produced. To investigate the optimal amount of the Ni@GRNT to modify the GCE, different volumes of 1.0 mg/mL Ni@GRNT solution were dropped onto the bare GCE surface and the corresponding DPV curves were recorded. Figure 3a shows that the maximum DPV current is achieved for the substrate prepared with $4.0 \text{ }\mu\text{L}$ of the Ni@GRNT drop-casted onto the GCE. Hence, $4.0 \text{ }\mu\text{L}$ of the Ni@GRNT was considered as the optimal amount for the succeeding experiments. The impact of CLZ adsorption onto the Ni@GRNT/GCE surface was also studied. Figure 3b shows the peak current versus adsorption time for 0.1 mmol L^{-1} CLZ in 0.1 mol L^{-1} PBS at $\text{pH}=7.0$. By increasing the accumulation/adsorption time from 0 to 350 s, the peak current was increased substantially. Also, after a preconcentration of 220 s, the current value plateaued (and after, declined a bit) due to the surface saturation of the electrode by the CLZ. As such, the optimum accumulation time is deemed to be at 220 s.

Effect of scan rate and pH

To investigate the kinetics and electrochemical behavior of the Ni@GRNT/GCE necessary for the CLZ detection, we also performed cyclic voltammetry with $1.0 \text{ }\mu\text{mol L}^{-1}$ CLZ in PBS ($\text{pH}=7.0$) from 50 to 500 mV s^{-1} (Fig. 4a). With increasing scan rate, both the I_{pa} and I_{pc} values increased in a linear manner (Fig. 4b) and can be described by the following equations:

$$I_{pa}(\mu\text{A}) = 0.0304 v + 1.8438, R^2 = 0.9954$$

$$I_{pc}(\mu\text{A}) = -0.024 v - 0.8114, R^2 = 0.995$$

These results show the adsorption process that could influence the electrochemical oxidation of CLZ. A linear behavior was also observed for the $\log I_{pa}$ versus $\log v$ with a slope of 0.7, providing the adsorption-controlled oxidation of the CLZ onto the Ni@GRNT/GCE [1, 35]. Also, by increasing the potential sweep rate, the peak potential (E_{pa}) value moved to more positive values, posing a kinetic limitation to the CLZ oxidation reaction. As can be seen

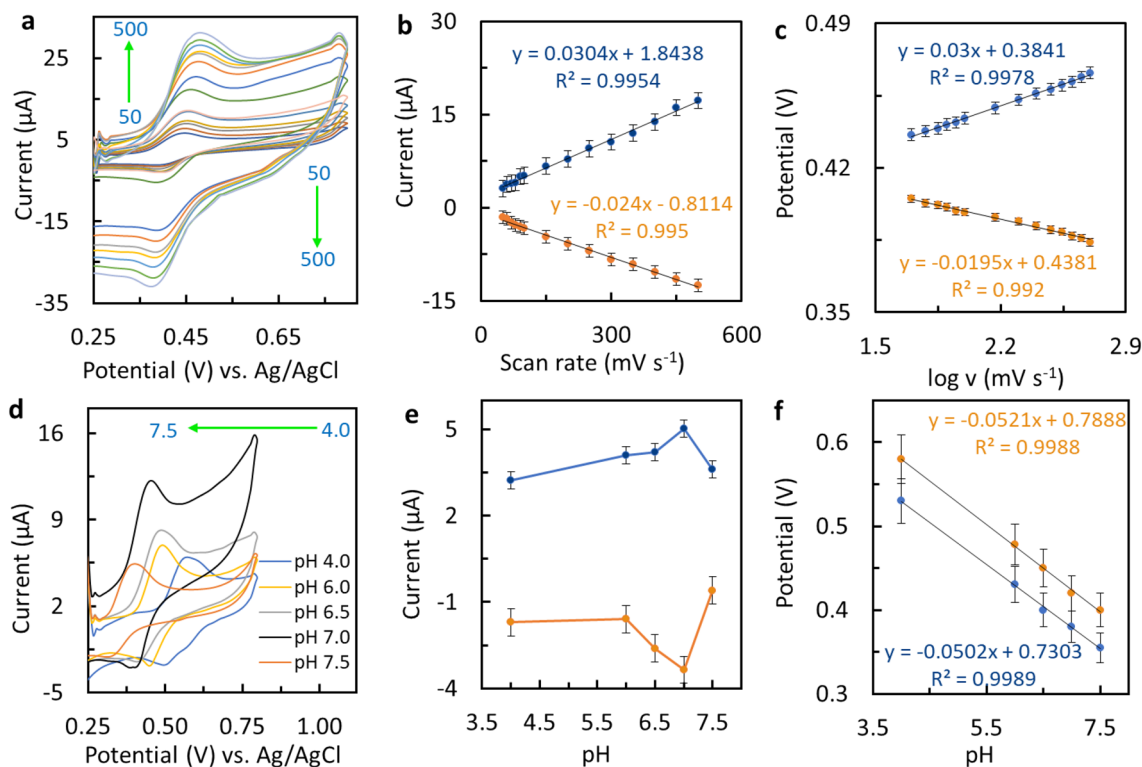
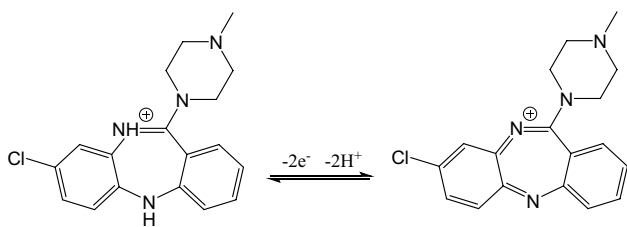


Fig. 4 **a** The CVs of $1.0 \mu\text{mol L}^{-1}$ CLZ on Ni@GRNT/GCE at pH=7.0 and at various scan rates (0–500 mV s^{-1}) (inner to outer curves). **b** Plot of current versus scan rate and **c** plot of peak potential versus log scan rate. **d** The CVs of $1.0 \mu\text{mol L}^{-1}$ CLZ on Ni@GRNT/

GCE in 0.1 mol L^{-1} PBS at different pH values (4.0, 6.0, 6.5, 7.0, and 7.5). **e** the correlation of the current value versus pH value and **f** peak potential vs. pH value corresponding to the CV (Number of replicates=4)



Scheme 2 The proposed mechanism for the electrochemical oxidation of CLZ on the Ni@GRNT/GCE surface

in Fig. 4c, a good linearity between the E_{pa} and $\log v$ can be seen:

$$E_{\text{pa}}(\text{V}) = 0.035 \log v + 0.3841, R^2 = 0.9978$$

$$E_{\text{pc}}(\text{V}) = -0.0195 \log v + 0.4381, R^2 = 0.992$$

The Tafel slope (b) was obtained from the slope of the equation [13, 35]:

$$E_{\text{pa}} = \frac{b}{2} \log v + \text{constant}$$

The slope of the Tafel plot was calculated to be 0.07, and considering the $2e^-$ oxidation of the CLZ on the Ni@GRNT/GCE surface, we obtained a transfer coefficient (α) value of 0.57, using the equation [16, 35]:

$$b = \frac{2.303/RT}{(1 - \alpha)nF}$$

where R is the ideal gas constant, T is temperature, n is the number of electrons (2 in a $2e^-$ reaction/process) and F is Faraday's constant ($96,485.3365 \text{ C mol}^{-1}$).

From these results and using the Laviron equation:

$$\begin{aligned} \text{Log } K_s &= \alpha \log (1 - \alpha) + (1 - \alpha) \log \alpha \\ &\quad - \log (RT / nFv) - \alpha (1 - \alpha) \\ &\quad (nF\Delta E_p / 2.3 RT) \end{aligned}$$

We calculated the catalytic rate constant (k_{cat}) [1, 35] to be 2.05 s^{-1} . This k_{cat} value points to the ability of the Ni@GRNT to promote the electron transfer between the CLZ and GCE surface effectively.

Additionally, the influence of pH on the electrochemical behavior of CLZ adsorbed on Ni@GRNT/GCE was also investigated. This was done in the range of 4.0–7.5 and in the

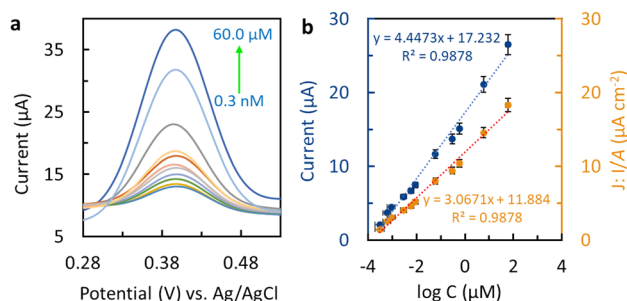


Fig. 5 **a** The DPVs of the Ni@GRNT/GCE for various concentrations of CLZ (0.3 nmol L⁻¹, 0.6 nmol L⁻¹, 0.9 nmol L⁻¹, 3.0 nmol L⁻¹, 6.0 nmol L⁻¹, 9.0 nmol L⁻¹, 30.0 nmol L⁻¹, 60.0 nmol L⁻¹, 0.6 µmol L⁻¹, 6.0 µmol L⁻¹, and 60.0 µmol L⁻¹). **b** The calibration plot of peak current versus CLZ concentration (blue curve) and current density versus the CLZ concentration (orange curve)

presence of 1.0 µmol L⁻¹ CLZ (Fig. 4d). The maximum peak current signal was obtained at pH = 7.0 (Fig. 4e). Plotting the E_{pa} versus pH gives a linear relation between the oxidation peak potential and pH (Fig. 4f). The equations for the peak potential versus pH linear relations are given below:

$$E_{pa}(V) = -0.0521 \text{ pH} + 0.7888, R^2 = 0.9988$$

$$E_{pc}(V) = -0.0502 \text{ pH} + 0.7303, R^2 = 0.9989$$

The decrease in E_p with increasing pH demonstrates the contribution of proton transfer in the oxidation reaction of CLZ. The slope is then equal to the Nernst slope, suggesting that the CLZ on the modified electrode surface in the pH range of 4.0–7.5 involves a two electron-two proton process, as postulated in Scheme 2 [1, 5 and 6].

Determination of the CLZ by Ni@GRNT/GCE

The DPV signals for several concentrations of the CLZ (from 0.3 to 60.0 µmol L⁻¹) were also measured to evaluate the ability of the Ni@GRNT/GCE in detecting and determining the CLZ level. The currents increase with increasing CLZ concentrations (Fig. 5a). The plot of the peak current against the CLZ concentration is linear within the measured concentration range:

$$I_{pa}(\mu A) = 4.4473 \log C(\mu \text{mol L}^{-1}) + 17.232, R^2 = 98.78$$

The detection limit (LOD) of the method based on a signal-to-noise ratio of 3 (S/N = 3) was calculated to be 0.1 nmol L⁻¹. In addition, sensitivity was also evaluated for an effective and easy means of comparing our sensor with those of other platforms, especially since this factor depends on the actual active surface area of the working electrode. We determined a value of 3.06 µA µmol L⁻¹ cm⁻² (Fig. 5b) for the sensitivity of our sensor.

Our results show that our simple, cost-effective, non-toxic and stable (in terms of signal response) platform for detecting CLZ and determining its concentration is comparable or even better than the other methods reported for CLZ detection (Table 1). These satisfactory results can be attributed to (i) the preparation of the active sites onto the modified GCE surface which led to an effective oxidation of CLZ; (ii) using the Ni@GRNT and taking advantage of its better conductivity and higher surface area; and (iii) the structure of Ni@GRNT tubes which allow them to be easily functionalized with other active materials simultaneously on both outer and inner tube surfaces to increase the electrochemical performance.

Table 1 Comparison of Ni@GRNT/GCE with other sensor electrodes for the detection of CLZ

Modified electrode	Technique	pH	Linear range (nmol L ⁻¹)	LOD (nmol L ⁻¹)	Potential (mV)	Real samples	References
BiCl ₃ /GCE	DPV	5.0	1.0 × 10 ⁺³ –1.0 × 10 ⁺⁴	6.1	320	Tablet	[36]
µFSE	Amperometry	–	1.0 × 10 ⁺² –1.0 × 10 ⁺⁴	24.0	–	Blood	[37]
TiO ₂ NP/CPE	DPV	9.0	5 × 10 ⁺² –45 × 10 ⁺³	61.0	370	Tablet	[5]
MWWTd/NCe/PPYf/GCE	LSV	5.44	1.0 × 10 ⁺¹ –5 × 10 ⁺³	3.0	500	Blood	[6]
MWWT/GCE	SWV	7.0	1.0 × 10 ⁺² –2.0 × 10 ⁺³	30	462	Urine and blood	[38]
CIL and ISS-CIL Electrodesa	DPV	3.5	1.0–1.0 × 10 ⁺²	0.20	570	Blood	[39]
Rug-TiO ₂ /CPE	SWV	10.4	9.0 × 10 ⁺² –4.0 × 10 ⁺⁴	0.43	210	Tablet and urine	[40]
TiO ₂ NP@CuO/CPE	DPV	5.0	1.0 × 10 ⁻³ –1.0 × 10 ⁺⁴	0.01	500	Blood and tablet	[1]
RuTiO ₂ /MWCNTs-CPE	SWV	5.0	10.0–70.0	0.05	480	Tablet and urine	[10]
NiO/GQD/GCE	DPV	2.0	3.0–1.0 × 10 ⁺³	0.55	~650	Blood and tablet	[41]
Ni@GRNT/GCE	DPV	7.0	0.3–6.0 × 10⁺⁴	0.1	410	Blood and tablet	This work

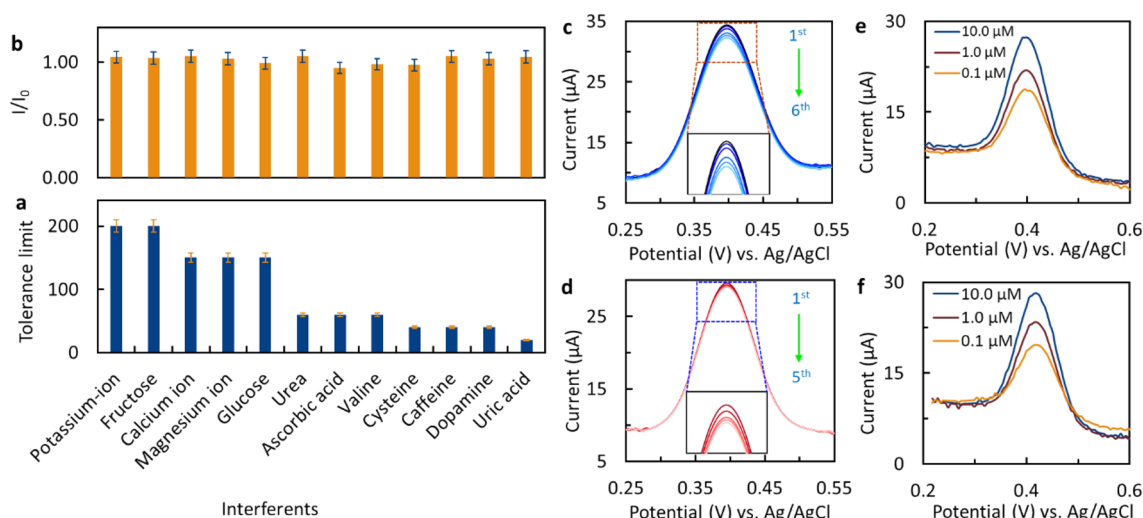


Fig. 6 **a** A histogram of the tolerance limit of the different interferents. The tolerance limit of the interferents added to $1.0 \mu\text{mol L}^{-1}$ CLZ was ~ 200 times for K^+ and fructose, ~ 150 times for Ca^{2+} , Mg^{2+} and glucose, ~ 60 times for urea, ascorbic acid, and valine, ~ 40 times for cysteine, caffeine, and dopamine, and ~ 20 times for uric acid. **b** The current ratio (I/I_0) for the different interferents (I and I_0 represent the peak current responses of CLZ in the presence and absence of

interference, respectively). **c** The recorded DPVs of the Ni@GRNT/GCE containing $20.0 \mu\text{mol L}^{-1}$ CLZ solution in PBS 0.1 mol L^{-1} in $\text{pH}=6.5$ for six days and signals were recorded every day **d** recording five replicate DPVs in PBS, $\text{pH} 6.5$ containing $5.0 \mu\text{mol L}^{-1}$ CLZ (number of replicates=3). DPVs for CLZ in the real samples **e** for CLZ tablets and **f** for human blood serum samples (Number of replicates=4)

Investigation of the selectivity

The impacts of several organic and inorganic species on CLZ measurement as probabilistic interferences were estimated to assess the applicability of the sensor for real sample analysis. The tolerance limit was defined as the concentration ratio of the CLZ in the presence of interferences which causes a relative error of $< \pm 5.0\%$. The results depicted that various interfering species did not interfere with the detection of $1.0 \mu\text{mol L}^{-1}$ CLZ. A histogram of the change of concentration versus several probable interferents against CLZ (Fig. 6a) indicates that $200 \mu\text{mol L}^{-1}$ of K^+ and fructose,

$150 \mu\text{mol L}^{-1}$ of Ca^{2+} , Mg^{2+} , and glucose, $60 \mu\text{mol L}^{-1}$ of urea, vitamin C, and valine, $40 \mu\text{mol L}^{-1}$ of cysteine, caffeine, and dopamine, and $20 \mu\text{mol L}^{-1}$ of uric acid (which are typical values of these species in human blood serum) did not significantly interfere with $1.0 \mu\text{mol L}^{-1}$ CLZ. Furthermore, a histogram of the current ratio (I/I_0) versus the interference (I and I_0 represent peak current responses of the CLZ in the presence and absence of interferents, respectively) was also plotted (Fig. 6b) to ensure that losses in the current response of the sensor due to the presence of interferents are acceptable.

Table 2 Determination of CLZ in tablet and human blood serum samples (the mean of four replicates)

Sample	No	As-prepared CLZ concentration (mol L^{-1}) *	Derived CLZ concentration from measurements (mol L^{-1}) **	Recovery (%)	Error (%)
Tablet	1	1.00×10^{-7}	1.06×10^{-7}	106.20	6.20
	2	1.00×10^{-6}	0.95×10^{-6}	95.10	4.90
	3	1.00×10^{-5}	0.97×10^{-5}	97.24	2.76
Serum	1	1.00×10^{-7}	0.93×10^{-7}	93.43	6.57
	2	1.00×10^{-6}	0.96×10^{-6}	96.27	3.73
	3	1.00×10^{-5}	0.98×10^{-5}	98.18	1.82

*Concentration value determined from the quantitative preparation of the sample (volumetric and gravimetric quantities)

**Concentration calculated and derived from DPV measurements

Long-term stability and repeatability of the sensor

Another important factor to consider in fabricating CLZ sensors is its stability. For this, we recorded the DPV peak current in $20.0 \mu\text{mol L}^{-1}$ CLZ every day for 6 days (Fig. 6c). The peak current responses of the Ni@GRNT/GCE on the last days were $91.0 \pm 3.5\%$ of the original peak current (day 1), indicating a standard deviation of 5.0%, which reflects an acceptable long lifetime of the sensor platform. The repeatability of the Ni@GRNT/GCE results was calculated by recording five replicate DPVs in PBS, pH 6.5 containing $5.0 \mu\text{mol L}^{-1}$ CLZ (Fig. 6d). The relative standard deviation (RSD) was estimated to be 2.1%, a satisfactory result showing the compatibility of the Ni@GRNT/GCE for CLZ sensing and further confirming that the sensor is extremely stable and can be used to obtain repeatable measurements.

Analytical application to measure CLZ in tablet and spiked human blood serum samples

The CLZ sensing in the spiked serum samples and tablet were performed to assess the reliability of the sensor in measuring CLZ concentrations in real samples. The DPVs were recorded in samples prepared via the standard addition method (Fig. 6e and f). The accuracy of the measurement was determined by comparing the concentrations derived from the DPV measurements with the added (known) concentrations based on the sample preparation. The good RSD and accuracy calculated from three replicate measurements at some nominal concentrations using the prepared sensor can be seen in Table 2. These results show the reliability of the method used and of the fabricated sensor, which can be used for the analysis of real samples giving adequate and satisfactory results for CLZ sensing.

Conclusion

Here, an electrochemical sensor based on the Ni@GRNT/GCE was used for CLZ measurement. The results show that the interesting physicochemical properties, good electrocatalytic activity, and high electrochemically active surface area of Ni@GRNT provide effective active sites for the fabrication of functionalized sensor for CLZ sensing. Moreover, the applicability of the fabricated sensor for real-sample CLZ sensing was investigated using CLZ tablets and spiked human blood serum samples. The results show the great potential of using Ni@GRNT/GCE in the fabricating electrochemical platforms for clinical use and quality control measurements, which can be extended to other target analytes.

Acknowledgements The authors would like to thank Dr. Christine Joy Querebillo for her helpful comments on improving the language of manuscript.

Funding Open Access funding enabled and organized by Projekt DEAL.

Declarations

Conflict of interest The authors declare that they have no known competing financial interests or personal relationships that could have appeared to influence the work reported in this paper. The authors declare the following financial interests/personal relationships which may be considered as potential competing interests:

Open Access This article is licensed under a Creative Commons Attribution 4.0 International License, which permits use, sharing, adaptation, distribution and reproduction in any medium or format, as long as you give appropriate credit to the original author(s) and the source, provide a link to the Creative Commons licence, and indicate if changes were made. The images or other third party material in this article are included in the article's Creative Commons licence, unless indicated otherwise in a credit line to the material. If material is not included in the article's Creative Commons licence and your intended use is not permitted by statutory regulation or exceeds the permitted use, you will need to obtain permission directly from the copyright holder. To view a copy of this licence, visit <http://creativecommons.org/licenses/by/4.0/>.

References

- M.H. Ghanbari, F. Shahdost-Fard, M. Rostami, A. Khoshroo, A. Sobhani-Nasab, N. Gholipour, H. Salehzadeh, M. Ganjali, M. Rahimi-Nasrabadi, F. Ahmadi, *Microchim. Acta* (2019). <https://doi.org/10.1007/s00604-019-3760-7>
- C. Frahnert, M. Rao, K. Grasmäder, *J. Chromatogr. B* (2003). [https://doi.org/10.1016/S1570-0232\(03\)00393-3](https://doi.org/10.1016/S1570-0232(03)00393-3)
- K. Farhadi, A. Karimpour, *Anal. Sci.* (2007). <https://doi.org/10.2116/analsci.23.479>
- N.Y. Hasan, M.A. Elkawy, B.E. Elzeany, N.E. Wagieh, *J. Pharm. Biomed. Anal.* (2002). [https://doi.org/10.1016/S0731-7085\(02\)00125-5](https://doi.org/10.1016/S0731-7085(02)00125-5)
- M.H. Mashhadizadeh, E. Afshar, *Electrochim. Acta* (2013). <https://doi.org/10.1016/j.electacta.2012.09.004>
- S. Shahrokhian, Z. Kamalzadeh, A. Hamzehloei, *Bioelectrochemistry* (2013). <https://doi.org/10.1016/j.bioelechem.2012.10.002>
- M.H. Ghanbari, A. Khoshroo, H. Sobati, M. Ganjali, M. Rahimi-Nasrabadi, F. Ahmadi, *Microchem. J.* (2019). <https://doi.org/10.1016/j.microc.2019.03.016>
- M.H. Ghanbari, P. Sharafi, S. Nayeboosadr, Z. Norouzi, *Microchim. Acta* (2020). <https://doi.org/10.1007/s00604-020-04529-8>
- A.S. Al Attas, *Int. J. Electrochem. Sci.* **4**, 9 (2009)
- N.P. Shetti, D.S. Nayak, S.J. Malode, R.M. Kulkarni, *ECS J. Solid State Sci. Tech* (2018). <https://doi.org/10.1149/2.0101807jss>
- M. Kang, E. Kim, T.E. Winkler, G. Banis, Y. Liu, C.A. Kitchen, D.L. Kelly, R. Ghodssi, G.F. Payne, *Biosens. Bioelectron.* (2017). <https://doi.org/10.1016/j.bios.2017.04.008>
- M.H. Ghanbari, Z. Norouzi, M.M. Ghanbari, *Microchem. J.* (2020). <https://doi.org/10.1016/j.microc.2020.104994>
- M.H. Ghanbari, Z. Norouzi, *Microchem. J.* (2020). <https://doi.org/10.1016/j.microc.2020.105098>

14. A. Shamsi, F. Ahour, Adv. J. Chem. Sect. A (2020). <https://doi.org/10.22034/AJCA.2020.252025.1215>
15. L.L. Shen, G.R. Zhang, W. Li, M. Biesalski, B.J. Etzold, ACS Omega (2017). <https://doi.org/10.1021/acsomega.7b00611>
16. M.H. Ghanbari, F. Shahdost-fard, A. Khoshroo, M. Rahimi-Nasrabadi, M. Ganjali, M. Wysokowski, T. Rebiš, S. Zóltowska-Aksamitowska, T. Jesionowski, P. Rahimi, Y. Joseph, H. Ehrlich, Microchim. Acta (2019). <https://doi.org/10.1007/s00604-019-3530-6>
17. D. Yu, L. Dai, J. Phys. Chem. Lett. (2010). <https://doi.org/10.1021/jz9003137>
18. H. Gao, F. Xiao, C.B. Ching, H. Duan, ACS Appl. Mater. Inter. (2012). <https://doi.org/10.1021/am302280b>
19. Y. Yang, N.D. Kim, V. Varshney, S. Sihm, Y. Li, A.K. Roy, J.M. Tour, J. Lou, Nanoscale (2017). <https://doi.org/10.1039/C6NR09897E>
20. V. Sridhar, I. Lee, H.H. Chun, H. Park, Carbon (2015). <https://doi.org/10.1016/j.carbon.2015.01.063>
21. V. Sridhar, H.J. Kim, J.H. Jung, C. Lee, S. Park, I.K. Oh, ACS Nano (2012). <https://doi.org/10.1021/nn3046133>
22. S.H. Lee, V. Sridhar, J.H. Jung, K. Karthikeyan, Y.S. Lee, R. Mukherjee, N. Koratkar, I.K. Oh, ACS Nano (2013). <https://doi.org/10.1021/nn4007253>
23. S. Vadahanambi, S.H. Lee, W.J. Kim, I.K. Oh, Environ. Sci. Tech. (2013). <https://doi.org/10.1021/es401389g>
24. Y. Zhu, L. Li, C. Zhang, G. Casillas, Z. Sun, Z. Yan, G. Ruan, Z. Peng, A.R.O. Raji, C. Kittrell, R.H. Hauge, J.M. Tour, Nat. Commun. (2012). <https://doi.org/10.1038/ncomms2234>
25. D.H. Lee, J.E. Kim, T.H. Han, J.W. Hwang, S. Jeon, S.Y. Choi, W.J. Lee, R.S. Ruoff, S.O. Kim, Adv. Mater. (2010). <https://doi.org/10.1002/adma.200903063>
26. C.L. Sun, S.Y. Lai, K.J. Tsai, J. Wang, J. Zhou, H.Y. Chen, Microchem. J. (2022). <https://doi.org/10.1016/j.microc.2022.107586>
27. F. Du, Z. Dong, F. Liu, S. Anjum, M. Hosseini, G. Xu, Electrochim. Acta (2022). <https://doi.org/10.1016/j.electacta.2022.140431>
28. C. Wei, J. Xiao, S. Liu, Z. Wang, L. Chen, W. Teng, Anal. Lett. (2022). <https://doi.org/10.1080/00032719.2021.2002887>
29. R. Liu, B. Li, F. Li, V. Dubovyk, Y. Chang, D. Li, K. Ding, Q. Ran, G. Wang, H. Zhao, Food Chem. (2022). <https://doi.org/10.1016/j.foodchem.2022.132573>
30. M.H. Ghanbari, F. Shahdost-Fard, H. Salehzadeh, M. Ganjali, M. Iman, M. Rahimi-Nasrabadi, F. Ahmadi, Microchim. Acta (2019). <https://doi.org/10.1007/s00604-019-3761-6>
31. M.H. Ghanbari, M.H. Mashhadizadeh, Z. Norouzi, J. Iran. Chem. Soc. (2020). <https://doi.org/10.1007/s13738-020-02114-7>
32. N.N. Nghia, Y.I. Lee, Microchim. Acta (2019). <https://doi.org/10.1007/s00604-018-3169-8>
33. M.H. Ghanbari, M.H. Mashhadizadeh, Z. Norouzi, H. Salehzadeh, Microchem. J. (2022). <https://doi.org/10.1016/j.microc.2022.107213>
34. X. Bao, J. Wang, X. Lian, H. Jin, S. Wang, Y. Wang, J. Mater. Chem. A (2017). <https://doi.org/10.1039/C7TA01240C>
35. A.J. Bard, L.R. Faulkner, H.S. White, *Electrochemical Methods: Fundamentals and Applications* (Wiley, Hoboken, 2022)
36. E. Gökmeşe, Ö.K. Yiğit, F.G. Gökmeşe, Hittite J. Sci. Eng. (2021). <https://doi.org/10.17350/HJSE19030000215>
37. M. Senel, A. Alachkar, Lab Chip (2021). <https://doi.org/10.1039/D0LC00970A>
38. M.R. Fathi, D. Almasifar, IEEE Sens. J. (2017). <https://doi.org/10.1109/JSEN.2017.2735304>
39. M. Arvand, M.G. Shiraz, Electroanalysis (2012). <https://doi.org/10.1002/elan.201100587>
40. N.P. Shetti, D.S. Nayak, S.J. Malode, R.M. Kulkarni, Sens. Actuator B (2017). <https://doi.org/10.1016/j.snb.2017.03.102>
41. A. Shamsi, F. Ahour, B. Sehatnia, J. Solid State Electrochem. (2018). <https://doi.org/10.1007/s10008-018-3982-3>